Electronic Supplementary Information for

Lattice-mismatch-induced growth of ultrathin Pt shells with high-index facets for boosting oxygen reduction catalysis

Xiang Li,[a]* Yaming Liu,[b] Wei Bi,[b] Jinglei Bi,[c] Ruiyun Guo,[b] Rui Li,[b] Chaoqi Wang,[b] Qi Zhan,[b] Weicong Wang,[b] Shengchun Yang[c], Fenglei Shi,[d] Jianbo Wu[d] and Mingshang Jin[b]*

[a] School of Materials and Chemical Engineering, Xi'an Technological University, Xi'an, Shaanxi 710021, China.

[b] Frontier Institute of Science and Technology and State Key Laboratory of Multiphase Flow in Power Engineering, Xi'an Jiaotong University, Xi'an, Shaanxi 710049, China.

[c] Key Laboratory of Shanxi for Advanced Materials and Mesoscopic Physics State Key Laboratory for Mechanical Behavior of Materials, School of Science, Xi'an Jiaotong University, Xi'an, Shaanxi 710049, China.

[d] State Key Laboratory of Metal Matrix Composites, School of Materials Science and Engineering, Shanghai Jiao Tong University, Shanghai 200240, China.

*To whom correspondence should be addressed. E-mail: jinm@mail.xjtu.edu.cn; xiangli2014@stu.xjtu.edu.cn.

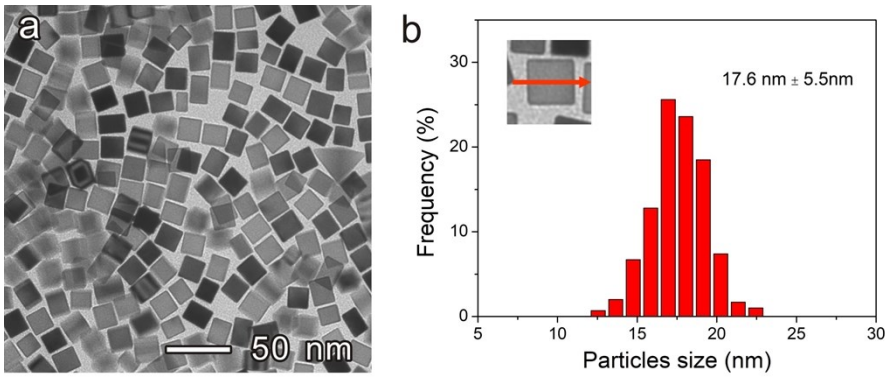

Figure S1. TEM image (a) and size distribution (b) of the original Pd nanocubes. The distance was measured along the red arrow of inset image.

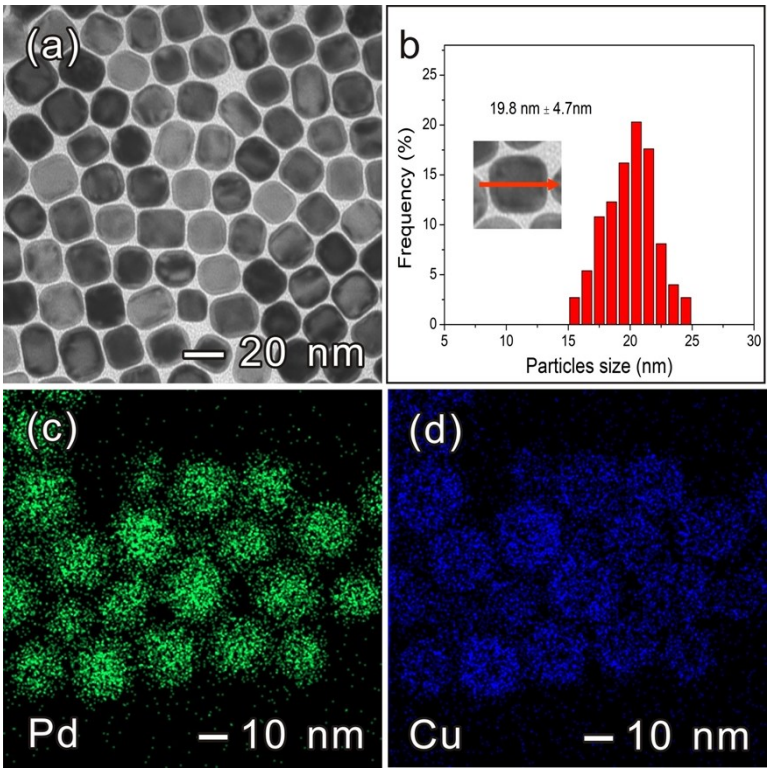

Figure S2. TEM image (a), size distribution (b), and element mapping (c, d) of the surface alloyed Pd-Cu nanocubes.

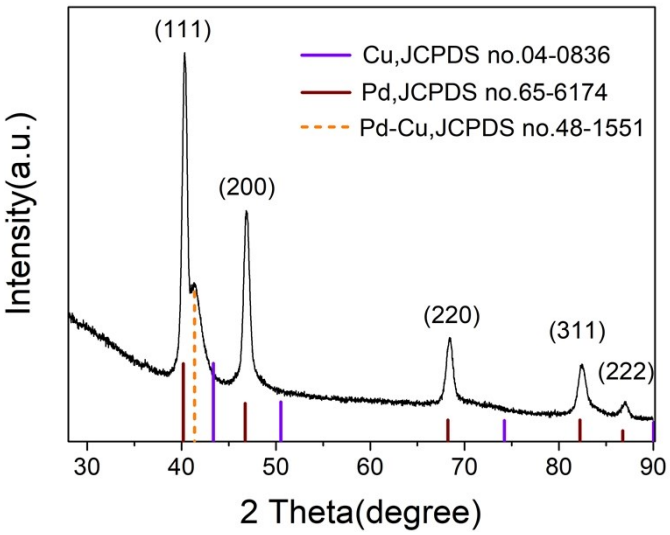

Figure S3. The XRD pattern of the surface alloyed Pd-Cu nanocubes.

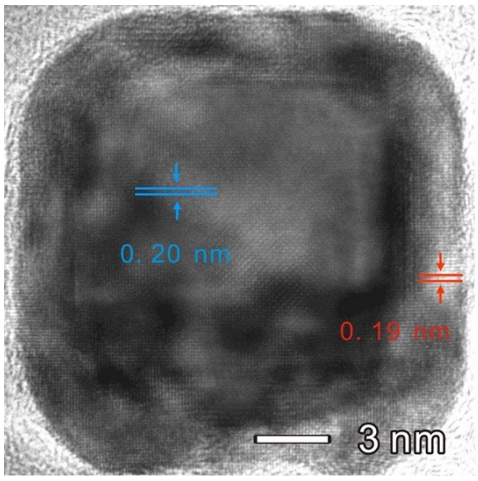

Figure S4. HRTEM image of the surface alloyed Pd-Cu nanocubes.

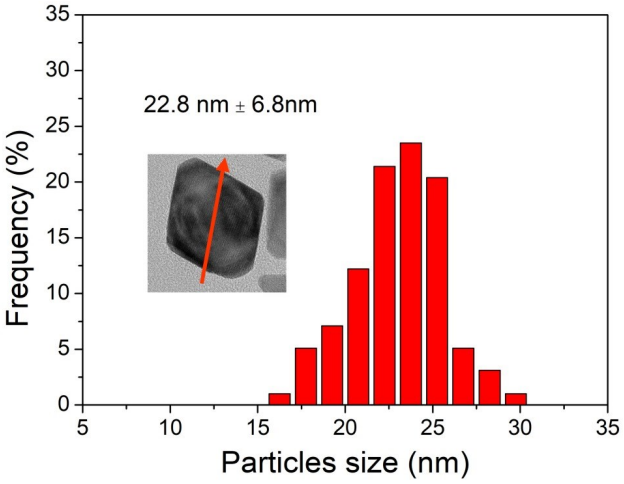

Figure S5. Size distribution of the Pd-Cu@Pt octahedral-like core-shell nanocrystals measured from the TEM image. The distance was measured along the red arrow of inset image.

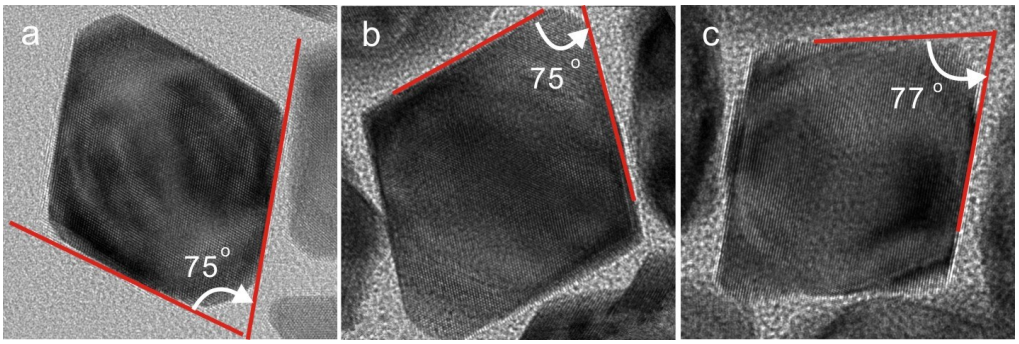

Figure S6. Angle Analysis of single octahedral-like Pd-Cu@Pt nanocrystal prepared through standard procedure.

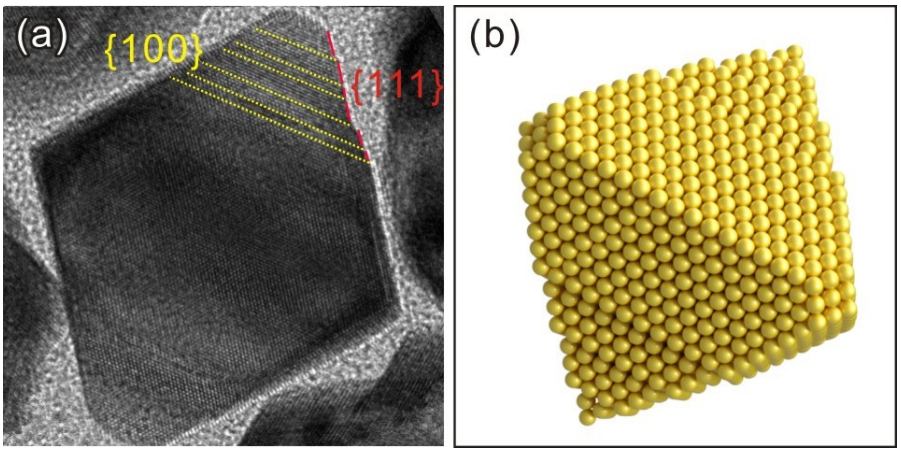

Figure S7. HRTEM image and the corresponding atomic model of a single octahedral-like Pd-Cu@Pt nanocrystal oriented along the [011] direction.

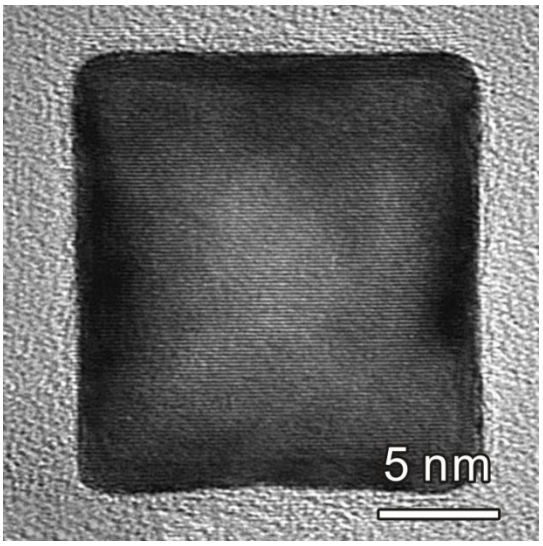

Figure S8. HRTEM image of the Pd@Pt nanocubes.

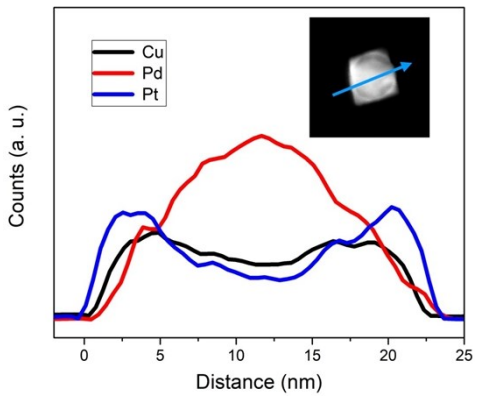

Figure S9. Elemental distribution by the EDX line scan analysis along the blue arrow in the insert image.

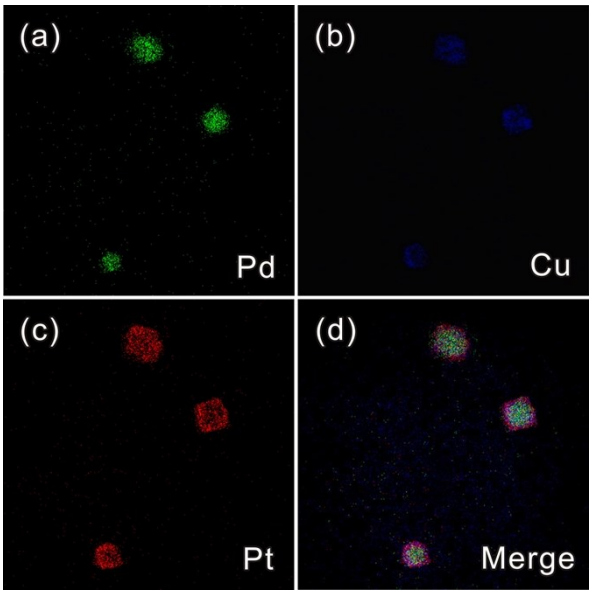

Figure S10. Energy-dispersive X-ray spectroscopy mapping of Pd, Cu, and Pt of octahedral-like Pd-Cu@Pt nanocrystal prepared through standard procedure except for that the reaction time is 3 hr.

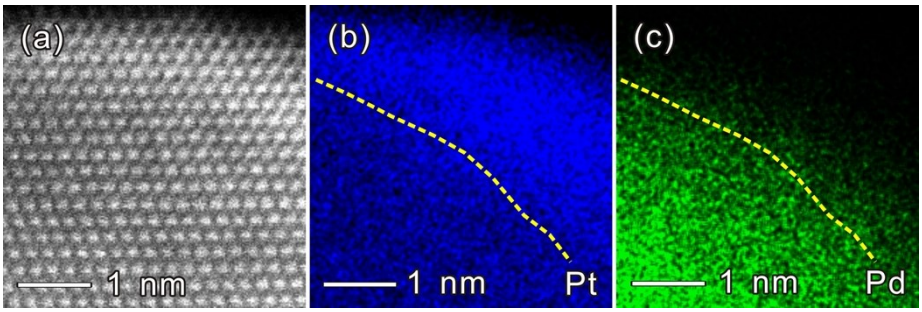

Figure S11. (a) High-resolution HAADF image of a surface region of PdCu@Pt nanocrystals. (b, c) Elemental mapping images, where the yellow dashed line denotes a possible boundary between the core and shell.

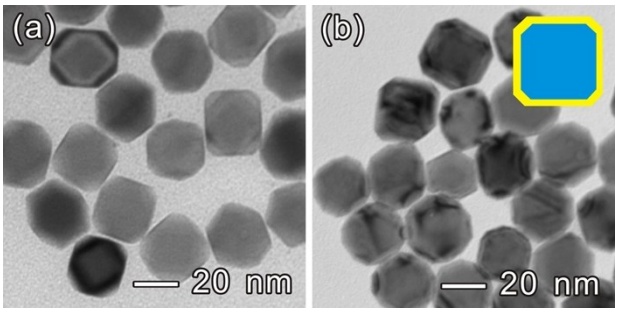

Figure S12. TEM images of the (a) truncated Pd nanocubes and (b) Pd@Pt nanocatalysts with the truncated Pd nanocubes as started seeds. The insert image of Figure b is corresponding model for Pd@Pt nanocrystal oriented along the [001] direction, with blue representing Pd while yellow Pt.

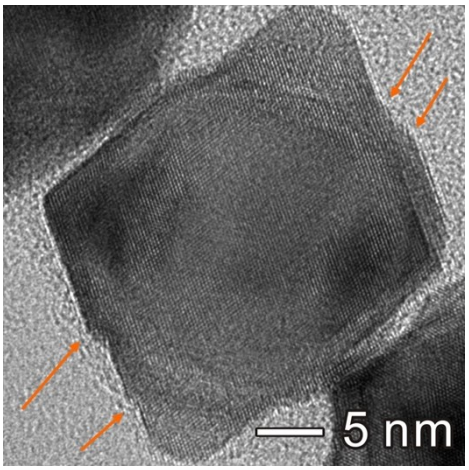

Figure S13. HRTEM image of an individual octahedral-like Pd-Cu@Pt nanocrystal prepared with the standard procedure except for that the reaction time was 3 hr.

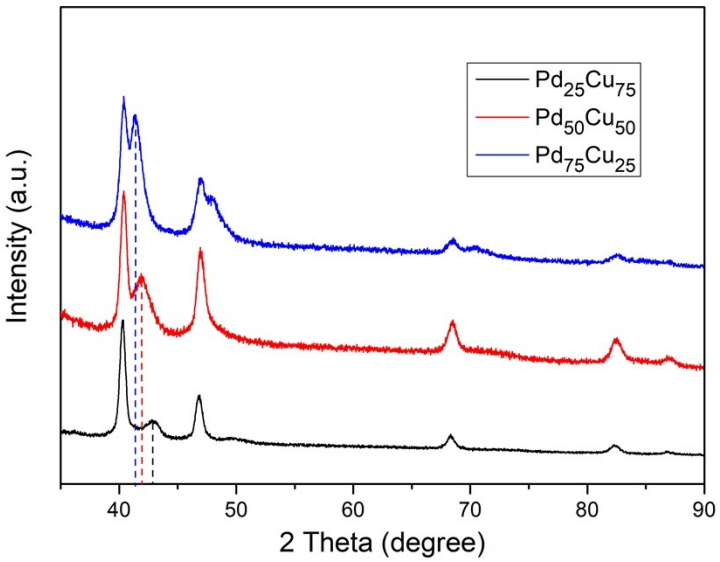

Figure S14. XRD patterns of Pd-Cu seeds with three different compositions.

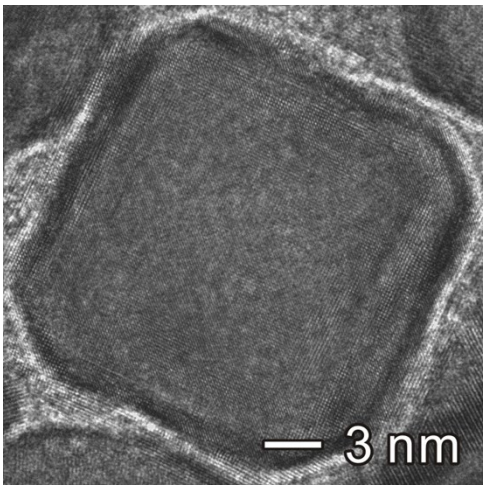

Figure S15. HRTEM image of an individual $Pd_{75}Cu_{25}$@Pt nanocrystals.

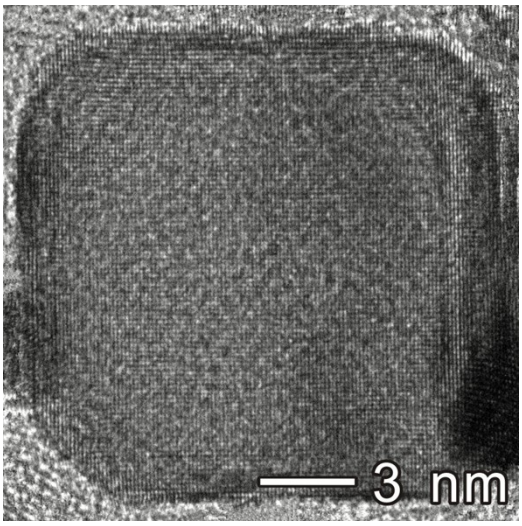

Figure S16. HRTEM image of an individual Pd-Cu@Pt nanocrystal prepared using the standard procedure except that the reaction was 0.5 hr.

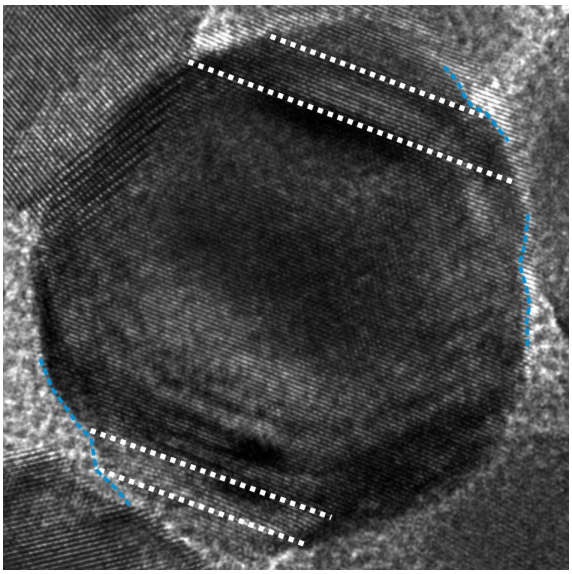

Figure S17. Surface structure of a single cuboctahedral-like Pd-Cu@Pt nanocrystal prepared through standard procedure except for that the reaction time is 1.5 hr.

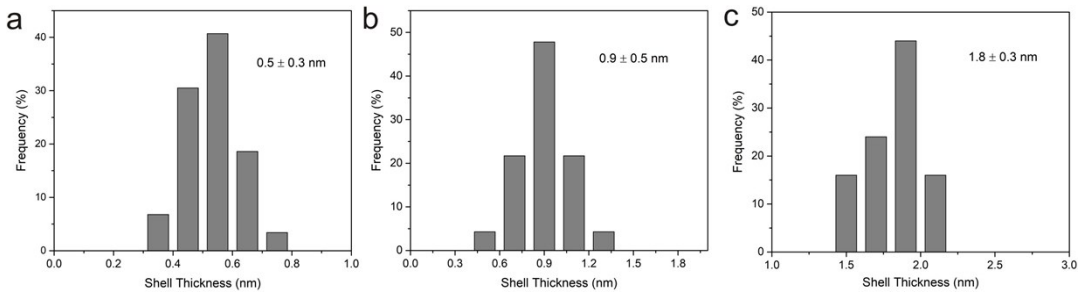

Figure S18. Histograms of Pt shell thicknesses of the Pd-Cu@Pt nanocrystals prepared at different reaction times along the [100] direction: (a) 0.5 hr, (b) 1.5 hr, (c) 3 hr.

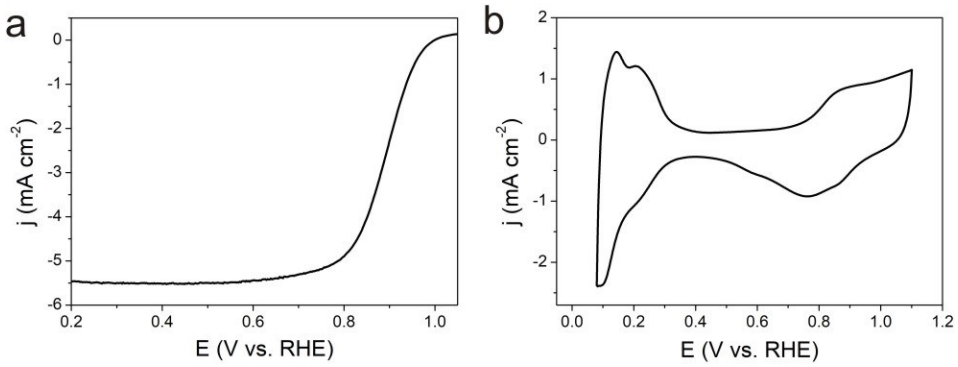

Figure S19. Electrochemical ORR properties of the commercial Pt/C catalysts. (a) ORR polarization curve for the catalysts at room temperature in O_2-saturated 0.1 M aqueous $HClO_4$ solutions at a sweep rate of 10 mV s^{-1} and rotation speed of 1600 rpm. (b) Cyclic voltammetry curve of the catalysts recorded at room temperature in N_2-purged 0.1 M aqueous $HClO_4$ solutions with a sweeping rate of 50 mV s^{-1}.

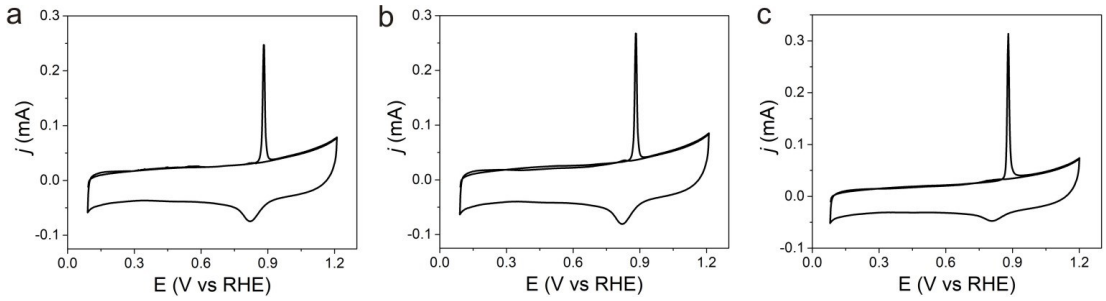

Figure. S20. CO-stripping curves of the Pd-Cu@Pt nanocatalysts that are obtained with different reaction times, (a) 0.5 hr, (b) 1.5 hr, (c) 3 hr. The catalyst surface was first saturated with CO by bubbling CO (99.9%) gas into the electrolyte (0.1 M aqueous $HClO_4$ solution) under open circuit potential for 25 min. The residual CO in the electrolyte was then removed by purging with Ar for 15 min. The CO-stripping curves were recorded with a scanning rate of 50 mV s^{-1} from 0.08 to 1.20 V (vs. RHE).

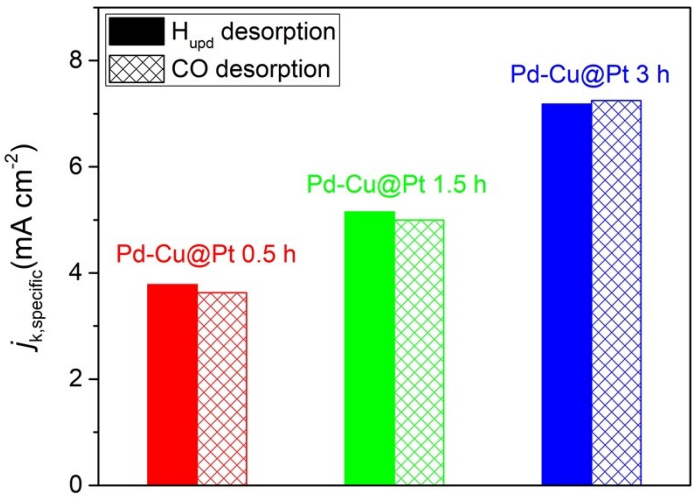

Figure S21. The specific activities of the catalysts given as kinetic current density (j_k) were normalized to the electrochemically active surface areas (ECSA). The ECSAs were derived from the charges responsible for the H_{upd} desorption and CO desorption, respectively.

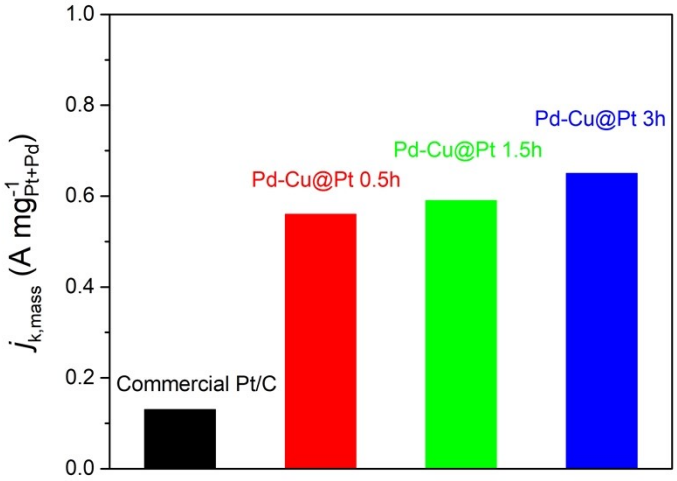

Figure S22. The total mass activity of Pt and Pd at 0.9 V vs reversible hydrogen electrode (RHE).

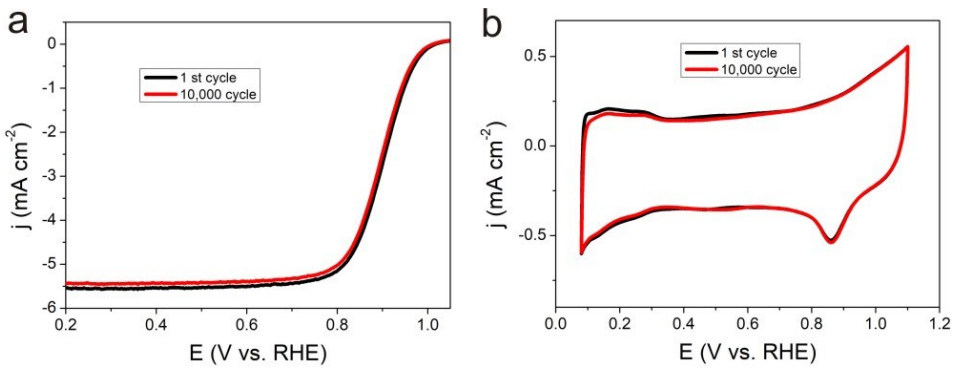

Figure S23. Stability of octahedral-like Pd-Cu@Pt nanocatalyst in electrocatalytic ORR. (a) ORR polarization curves of the catalyst before and after accelerated durability test. (b) CV curves of the catalyst before and after accelerated durability test.

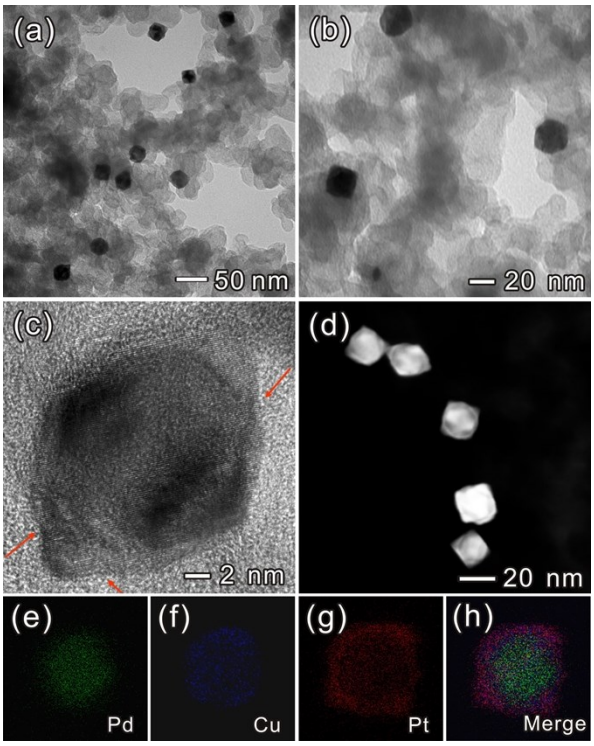

Figure S24. TEM characterizations of the octahedral-like Pd-Cu@Pt nanocatalysts after 10,000 cycles of potential sweeps in the ORR. (a) low-magnification TEM image, (b) high-magnification TEM image, (c) HRTEM image, (d) HAADF-STEM image, and (e-h) Energy-dispersive X-ray spectroscopy mapping.

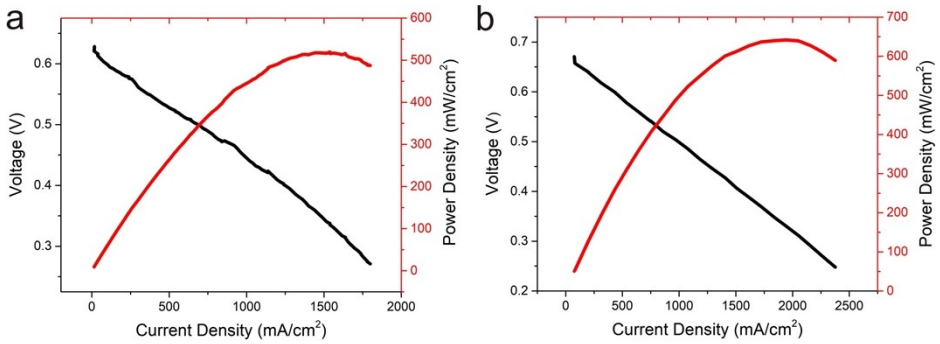

Figure S25. Fuel cell performance tested with the standard procedure except for that the backpressure was 120 KPa and the metal loadings was 0.5 mg_{Pt} cm^{-2} for cathode.

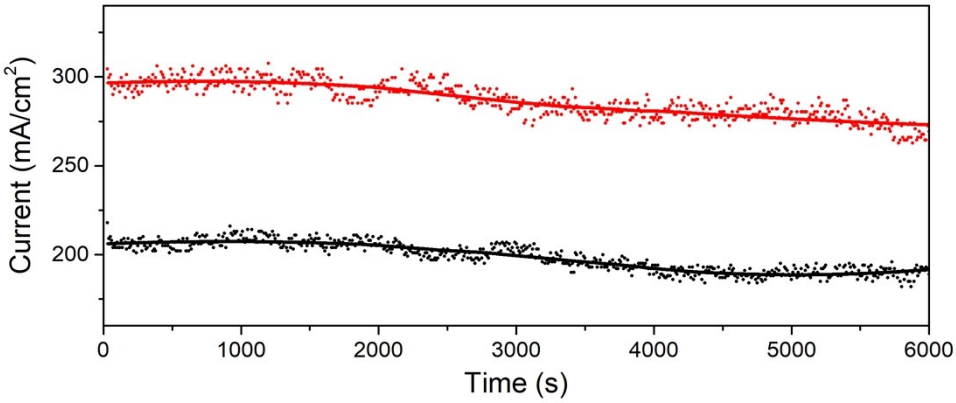

Figure S26. CA plots displaying the catalyst stability in FCs at 80 °C for Pd-Cu@Pt (red) and commercial Pt/C (black), which was performed at the potential corresponding to the maximum power output for 6000 s.

Table S1. The contents of Pt, Pd and Cu in Pd-Cu@Pt catalysts which are prepared with different times.

Samples		Pd-Cu@Pt 0.5 hr	Pd-Cu@Pt 1.5 hr	Pd-Cu@Pt 3 hr
The weight percentage (wt%) of metal calculated from the ICP data	Pd	54.8	51.2	47.9
	Cu	19.8	18.6	17.3
	Pt	25.4	30.2	34.8

Table S2. Specific ECSAs of the different type of the Pd-Cu@Pt nanocatalysts. Derived from the charges responsible for the H_{upd} and CO desorption respectively.

Samples		Pd-Cu@Pt 0.5 hr	Pd-Cu@Pt 1.5 hr	Pd-Cu@Pt 3 hr
Specific ECSA ($m^2\ g_{Pt}^{-1}$)	H_{upd} desorption	36.7	33.2	29.8
	CO desorption	38.3	34.2	29.5

Table S3. Comparison of the oxygen reduction reaction (ORR) electrocatalytic performance of Pt nanoshells with high-density steps with other materials with similar composition and architecture for ORR at 0.9 V versus RHE in acidic electrolyte (0.1 M $HClO_4$) published in recent years.

Catalysts	Mass activity ($A\ mg_{Pt}^{-1}$)	Specific activity ($mA\ cm^{-2}$)	References
Our catalyst	2.14	7.18	This work
PtPb/Pt	4.3	7.8	[1]
Porous PdCu@Pt	2.8	1.19	[2]
PdCu@PtCu	2.55	4.33	[3]
Pd@Pt-Ni	2.5	2.7	[4]
CoPt/Pt	2.26	8.26	[5]
PtFe@Pt	2.11	4.34	[6]
PtPb/PtNi	1.92	5.16	[7]
Pd_3Co/Pt	1.56	0.80	[8]
Pd@Pt Concave Decahedra	1.60	1.66	[9]
AuNi@Pt	1.52	1.18	[10]
Pd@Pt Icosahedra	1.36	0.83	[11]
Pt-Based Icosahedral Nanocages	1.28	3.50	[12]
Pt-Enriched Nanocage	1.12	2.48	[13]
Pd@Pt Octahedra	1.05	1.51	[14]

Au@Pt	0.94	1.09	[15]
Pd@PtNi	0.79	0.45	[16]
Pt-based Octahedral Nanocages	0.75	1.98	[17]
AuCu@Pt	0.57	-	[18]
$PdCu_5$@Pt	0.45	-	[19]
PtBi@Pt	0.36	1.04	[20]
Pd@Pt Nanocube	0.34	0.33	[21]
$PtNi_3$/Pt	0.29	1.49	[22]

Table S4. Specific ECSAs of the Pt/C catalyst and different type of the Pd-Cu@Pt nanocatalysts.

Samples		Commercial Pt/C	Pd-Cu@Pt 0.5 hr	Pd-Cu@Pt 1.5 hr	Pd-Cu@Pt 3 hr
Specific ECSA (m^2 g_{Pt}^{-1})	**1st cycle**	58	36.7	33.2	29.8
	After 10,000 cycles	28	26.1	27.9	27.6

Table S5. ORR performances of the Pt/C catalyst and different types of the Pd-Cu@Pt nanocatalysts.

Catalysts	The first cycle		After 10,000 cycles	
	$J_{k,mass}$ ($A\ mg_{Pt}^{-1}$)	$J_{k,specific}$ ($mA\ cm^{-2}$)	$J_{k,mass}$ ($A\ mg_{Pt}^{-1}$)	$J_{k,specific}$ ($mA\ cm^{-2}$)
Commercial Pt/C	0.13	0.22	0.068	0.24
Pd-Cu@Pt 0.5 hr	1.39	3.78	0.85	3.26
Pd-Cu@Pt 1.5 hr	1.71	5.15	1.33	4.76
Pd-Cu@Pt 3 hr	2.14	7.18	1.88	6.81

Table S6. Full cell performances of the Pt/C catalyst and Pd-Cu@Pt nanocatalysts.

PEMFC	Commercial Pt/C			Pd-Cu@Pt		
	40 ° C	*60* ° C	*80* ° C	*40* ° C	*60* ° C	*80* ° C
Open circuit voltages (V)	0.24	0.29	0.45	0.36	0.46	0.56
The maximum power (mW cm^{-2})	8.1	14.5	49.3	19.7	54.7	86.1
The corresponding voltages (V)	0.11	0.15	0.24	0.18	0.26	0.31

References

1. Bu, L.; Zhang, N.; Guo, S.; Zhang, X.; Li, J.; Yao, J.; Wu, T.; Lu, G.; Ma, J.; Su, D.; Huang, X. Biaxially Strained PtPb/Pt Core/Shell Nanoplate Boosts Oxygen Reduction Catalysis. *Science* **2016**, 354, 1410-1414.
2. Shao, M.; Shoemaker, K.; Peles, A.; Kaneko, K.; Protsailo, L. Pt Monolayer on Porous Pd-Cu Alloys as Oxygen Reduction Electrocatalysts. *J. Am. Chem. Soc.* **2010**, 132, 9253-9255.
3. Wang, C.; Sang, X.; Gamler, J..; Chen, D.; Unocic, R..; Skrabalak, S. Facet-Dependent Deposition of Highly Strained Alloyed Shells on Intermetallic Nanoparticles for Enhanced Electrocatalysis. *Nano Lett.* **2017**, 17, 5526-5532.
4. Choi, S.; Shao, M.; Lu, N.; Ruditskiy, A.; Peng, H.; Park, J.; Guerrero, S.; Wang, J.; Kim, M.; Xia, Y. Synthesis and Characterization of Pd@Pt-Ni Core-Shell Octahedra with High Activity toward Oxygen Reduction. *ACS Nano* **2014**, 8, 10363-10371.
5. Li, J.; Sharma, S.; Liu, X.; Pan, Y.; Spendelow, J.; Chi, M.; Jia, Y.; Zhang, P.; Cullen, D.; Xi, Z.; Lin, H.; Yin, Z.; Shen, B.; Muzzio, M.; Yu, C.; Kim, Y.; Peterson, A.; More, K.; Zhu, H.; Sun, S. Hard-Magnet $L1_0$-CoPt Nanoparticles Advance Fuel Cell Catalysis. *Joule* **2019**, 3, 124-135.
6. Luo, M.; Sun, Y.; Zhang, X.; Qin, Y.; Li, M.; Li, Y.; Li, C.; Yang, Y.; Wang, L.; Gao, P.; Lu, G.; Guo, S. Stable High-Index Faceted Pt Skin on Zigzag-Like PtFe Nanowires Enhances Oxygen Reduction Catalysis. *Adv. Mater.* **2018**, 30, 1705515.
7. Bu, L.; Shao, Q.; E, B.; Guo, J.; Yao, J.; Huang X. PtPb/PtNi Intermetallic Core/Atomic Layer Shell Octahedra for Efficient Oxygen Reduction Electrocatalysis. *J. Am. Chem. Soc.* **2017**, 139, 9576-9582.
8. Wang, J.; Inada, H.; Wu, L.; Zhu, Y.; Choi, Y.; Liu, P,; Zhou, W.; Adzic, R. Oxygen Reduction on Well-Defined Core-Shell Nanocatalysts: Particle Size, Facet, and Pt Shell Thickness Effects. *J. Am. Chem. Soc.* **2009**, 131, 17298-177302.
9. Wang, X.; Vara, M.; Luo, M.; Huang, H.; Ruditskiy, A.; Park, J.; Bao, S.; Liu, J.; Howe, J.; Chi, M.; Xie, Z.; Xia, Y. Pd@Pt Core-shell Concave Decahedra: A Class of Catalysts for the Oxygen Reduction Reaction with Enhanced Activity and Durability. *J. Am. Chem. Soc.* **2015**, 137, 15036-15042.
10. Chen, G.; Kuttiyiel, K.; Su, D.; Li, M.; Wang, C.; Buceta, D.; Du, C.; Gao, Y.; Yin, G.; Sasaki, K.; Vukmirovic, M.; Adzic, R. Oxygen Reduction Kinetics on Pt Monolayer Shell Highly Affected by the Structure of Bimetallic AuNi Cores. *Chem. Mater.* **2016**, 28, 5274-5281.

11. Wang, X.; Choi, S. I.; Roling, L. T.; Luo, M.; Ma, C.; Zhang, L.; Chi, M.; Liu, J.; Xie, Z.; Herron, J. A.; Mavrikakis, M.; Xia, Y. Palladium-Platinum Core-Shell Icosahedra with Substantially Enhanced Activity and Durability towards Oxygen Reduction. *Nat. Commun.* **2015**, 6, 7594.
12. Wang, Xue.; Figueroa-Cosme, L.; Yang, X.; Luo, M.; Liu, J.; Xie, Z.; Xia, Y. Pt-Based Icosahedral Nanocages: Using a Combination of {111} Facets, Twin Defects, and Ultrathin Walls to Greatly Enhance Their Activity toward Oxygen Reduction. *Nano Lett.* **2016**, 16, 1467-1471.
13. He, D. S.; He, D.; Wang, J.; Lin, Y.; Yin, P.; Hong, X.; Wu, Y.; Li, Y. Ultrathin Icosahedral Pt-Enriched Nanocage with Excellent Oxygen Reduction Reaction Activity. *J. Am. Chem. Soc.* **2016**, 138, 1494-1497.
14. Zhou, M.; Wang, H.; Vara, M.; Hood, Z.; Luo, M.; Yang, T.; Bao, S.; Chi, M.; Xiao, P.; Zhang, Y.; Xia Y. Quantitative Analysis of the Reduction Kinetics Responsible for the Onepot Synthesis of Pd-Pt Bimetallic Nanocrystals with Different Structures. *J. Am. Chem. Soc.* **2016**, 138, 12263-12270.
15. Bian, T.; Zhang, H.; Jiang, Y.; Jin, C.; Wu, J.; Yang, H.; Yang, D. Epitaxial Growth of Twinned Au-Pt Core-Shell Star-Shaped Decahedra as Highly Durable Electrocatalysts. *Nano Lett.* **2015**, 15, 7808-7815.
16. Zhao, X.; Chen, S.; Fang, Z.; Ding, J.; Sang, W.; Wang, Y.; Zhao, J.; Peng, Z.; Zeng, J. Octahedral Pd@$Pt_{1.8}$Ni Core-Shell Nanocrystals with Ultrathin PtNi Alloy Shells as Active Catalysts for Oxygen Reduction Reaction. *J. Am. Chem. Soc.* **2015**, 137, 2804-2807.
17. Zhang, L.; Roling, L. T.; Wang, X.; Vara, M.; Chi, M. F.; Liu, J. Y.; Choi, S.; Park, J.; Herron, J. A.; Xie, Z.; Mavrikakis, M.; Xia, Y. Platinum-Based Nanocages with Subnanometer-Thick Walls and Well-Defined, Controllable Facets. *Science* **2015**, 349, 412-416.
18. Yang, J.; Chen, X.; Yang, X.; Ying, J. Stabilization and compressive strain effect of AuCu core on Pt shell for oxygen reduction reaction. *Energy Environ. Sci.* **2012**, 5, 8976-8981.
19. Cochell, T.; Manthiram, A. *Langmuir*, **2012**, 28, 1579-1587.
20. Qin, Y.; Luo, M.; Sun, Y.; Li, C.; Huang, B.; Yang, Y.; Li, Y.; Wang, L.; Guo, S. Intermetallic hcp-PtBi/fcc-Pt Core/Shell Nanoplates Enable Efficient Bifunctional Oxygen Reduction and Methanol Oxidation Electrocatalysis. *ACS Catal.* **2018**, 8, 5581-5590.
21. Xie, S.; Choi, S. I.; Lu, N.; Roling, L. T.; Herron, J. A.; Zhang, L.; Park, J.; Wang, J.; Kim, M. J.; Xie, Z.; Mavrikakis, M.; Xia, Y. Atomic Layer-by-Layer Deposition of Pt on Pd

Nanocubes for Catalysts with Enhanced Activity and Durability toward Oxygen Reduction. *Nano Lett.* **2014**, 14, 3570-3576.

22. Haschᵉ, F,; Oezaslan, M.; Strasser, P. Activity, Structure and Degradation of Dealloyed PtNi3 Nanoparticle Electrocatalyst for the Oxygen Reduction Reaction in PEMFC. *J. Electrochem. Soc.* **2012**, 159, B24-B33.